Journal of Applied Polymer Science

Synergistic effect of aluminium phosphate and tungstophosphoric acid on the physicochemical properties of sulfonated poly ether ether ketone nanocomposite membrane

Soma Banerjee,[1] Kamal K. Kar[1,2]

[1]Advanced Nanoengineering Materials Laboratory, Materials Science Programme, Indian Institute of Technology Kanpur, Kanpur 208016, India

[2]Department of Mechanical Engineering, Indian Institute of Technology Kanpur, Kanpur 208016, India

Correspondence to: K. K. Kar (E-mail: kamalkk@iitk.ac.in)

ABSTRACT: This study explores the synergistic effect of aluminium phosphate (ALP) nanoparticles and tungstophosphoric acid (TPA) on the physicochemical properties of sulfonated poly ether ether ketone (SPEEK) nanocomposite membranes. SPEEK/TPA/ALP nanocomposite containing optimum TPA (10 wt %) and varying ALP content (3–10 wt %) are fabricated to investigate the effect of ALP nanoparticles on membrane properties. Experimental results reveal that nanocomposite membrane containing 3 wt % ALP nanoparticles and 10 wt % TPA exhibits 3.3 and 18.8 times higher proton conductivity compared to 10 wt % TPA filled SPEEK composite membrane and reference SPEEK membrane. ALP nanoparticles help in retaining water within the membranes and thus 59.4% reduction in water desorption rate is achieved compared to SPEEK/TPA membrane. The leaching of TPA is reduced by 34.5% which helps in retaining membrane properties. Membranes are thermally stable up to 200°C. Microstructure of the composite films is investigated by scanning electron microscope. © 2015 Wiley Periodicals, Inc. J. Appl. Polym. Sci. **2016**, *133*, 42952.

KEYWORDS: batteries and fuel cells; composites; membranes; properties and characterization; thermogravimetric analysis

Received 20 April 2015; accepted 16 September 2015
DOI: 10.1002/app.42952

INTRODUCTION

Fuel cells are the green and efficient means of energy, which have been vastly explored in recent decade owing to their immense potential in low energy stationary, transport, and portable applications. Polymer electrolyte membrane or proton exchange membrane (PEM) is one of the key elements of fuel cell devices, which selectively allows transport of protons from one side of the membrane electrode assembly (MEA) to other and keeps the device functional by simultaneous generation of heat and electricity. Perfluorinated polymer based membrane (e.g., Nafion®) is the most successful PEM till date in the field of fuel cell technology. However, due to functional and economical shortcomings of perfluorinated polymers, research is mainly dedicated to the development of cheap and efficient alternative PEMs.[1–4] Poly ether ether ketone (PEEK) has been the commonly functionalized polymer due to its exceptional thermal and chemical stability and easy processability.[5] In this direction, sulfonated poly ethers and polysulfones based PEMs were investigated by several researchers.[6–8] Sulfonated poly ether ether ketone (SPEEK) was the most commonly studied alternative PEM owing to its low cost and flexibility in functionalization. Although SPEEK was most commonly used polymer for PEMs; however, extensive swelling at high degree of sulfonation (DS) makes it mechanically unstable for fabrication of MEA. Nevertheless, efficiency of SPEEK was observed to decrease with prolonged operation time due to dehydration, which further motivated the researchers to develop alternate membrane.

SPEEK were often mixed with proton conducting and hydrophilic fillers to modify its ionic conductivity, water retention behavior, methanol permeability, as well as mechanical properties. Heteropolyacids (HPAs) were extensively utilized as solid conducting fillers due to availability of large numbers of conducting protons within them.[9–15] Hydrophilic fillers such as metal oxides (e.g., silica, titania), functionalized metal oxides,[16] clay,[17] aluminium phosphate (ALP),[18] zeolites,[19–21] zirconium phosphate,[19] etc. were used to modify water retention behavior of the SPEEK membranes. Silica particles were chemically modified by sulfonation, carboxylation, and phosphonation to improve water retention behavior as well as compatibility between filler and polymer matrix.[22] There were also report on organically modified titania

(containing hydrophilic and hydrophobic functionality) based SPEEK composite membranes.[23] Hydrophilic functionalization of titania nanoparticles led to enhanced proton conductivity in the composite membrane due to higher water up take capacity of functionalized nanoparticles, while hydrophobic functional groups helped in homogeneous distribution of the nanoparticles within SPEEK matrix.

SPEEK containing silicotungstic acid modified montmorillonite (STA-MMT) was also reported in the literature.[9] Addition of clay improved water uptake capacity of the composite membranes. Leaching of HPAs was reduced significantly due to immobilization of conducting fillers within the clay layers. Zeolite and zirconium phosphate based nanocomposite membranes were studied by Tripathi *et al.*[19] Use of nanofillers in combination improved mechanical strength, thermal and oxidative stability, water retentive properties, and dimensional stability of the nanocomposite PEMs. Functionalized and nonfunctionalized mesoporous hydrophilic filler based Nafion® and polymethylmethacrylate (PMMA)/ionic liquid composite membranes were also investigated and reported to exhibit superior proton conductivity compared to the nonporous filler based composite membranes due to better water retention within the porous structure.[24,25]

Like other hydrophilic fillers, porous nature of ALP makes them capable to show typical molecular sieves like behavior and therefore water retention for longer duration is expected in the nanocomposite membrane. Hence membrane can perform better without much loss in proton conductivity. ALP filled SPEEK composite membrane was also studied by Rangasamy *et al.*[18] Although there are extensive literatures on SPEEK composite membrane containing either solid proton conductor (e.g., tungstophosphoric acid, TPA) or hydrophilic fillers (e.g., metal oxides), however, there are only few cases, where the synergistic effect of multi-filled system have been studied.[26–29] Therefore it is considered worthwhile to study the synergistic effect of proton conducting filler (TPA) and hydrophilic filler (ALP) on the functional properties of SPEEK nanocomposite membranes. The porous ALP nanoparticles were synthesized by ultrasonic assisted co-precipitation in presence of citric acid.[30] SPEEK/TPA composite membranes were optimized for TPA content by fabricating composite membranes with varying percentage (5–50 wt %) of TPA to achieve highest proton conductivity. Finally, SPEEK/TPA/ALP nanocomposite membranes containing different ALP nanoparticles content (3–10 wt %) were fabricated by solution casting using optimum TPA (10 wt %). Control SPEEK and composite membranes containing different TPA or ALP were also prepared for comparison purposes. PEMs were characterized for ion exchange capacity (IEC), water uptake behavior, thermal stability, water retention ability, proton conductivity, etc. Effect of ALP on the leaching of conducting TPA was also studied using UV–vis spectroscopy. Morphology of membrane was investigated by scanning electron microscopy. Correlation was made between the microstructure and functional properties of membranes. To the best of our knowledge this study is the first experimental evidence of synergistic effect of TPA and ALP on the proton conductivity of SPEEK nanocomposite membrane for fuel cell application.

EXPERIMENTAL

Materials

Victrex PEEK was received from Victrex USA Inc. Sodium chloride and hydrochloric acid (HCl) were obtained from Qualigens fine chemicals. Dimethylacetamide (DMAc), TPA, ethylene glycol, methanol, and aluminium nitrate ($Al(NO_3)_3$) were received from Loba chemie. Sodium hydroxide (NaOH) and concentrated sulfuric acid were obtained from Samir tech-chem pvt. Ltd. and Fisher scientific. Diammonium hydrogen phosphate was received from s d fine-chem Ltd. All chemicals were used as such without further purification.

Synthesis of SPEEK

Synthesis of SPEEK was carried out according to the experimental method described in earlier study.[31] Initially PEEK powders were dried for 12 h at 100°C to eliminate the moisture. Dried PEEK was dissolved slowly in concentrated H_2SO_4 by means of magnetic stirring for 2 h at ambient temperature. In the subsequent step, temperature of PEEK solution was raised to 50°C and kept constant for 3 h to complete the sulfonation process. After desired time period, sulfonated polymer was discharged slowly into ice cold water under constant stirring to get shredded SPEEK. Finally SPEEK was washed repetitively with deionized water till neutral pH and dried in an oven at 60°C for 6 h and stored in a desiccator.

Synthesis of ALP Nanoparticles

The ALP nanoparticles were synthesized by sol-gel according to the procedure described in literature.[18] In a typical method 25 ml 0.25 M $Al(NO_3)_3$ solution was prepared in a 250 ml beaker and 1.313 g citric acid was added into it. In the subsequent step 25 ml 0.25 M diammonium hydrogen phosphate solution was dropped into the above mixture under continuous stirring and ultrasonication. Citric acid acted as a chelating agent and helped in binding of Al^{3+} with PO_4^{3-} in the reaction mixture. Afterwards 1.5 ml ethylene glycol was added into the above mixture (citric acid and ethylene glycol molar ratio was 1 : 4). The mixture was then heated slowly at 90°C to obtain highly viscous gel by evaporation of water. Brownish powder was obtained by heating the gel at 350°C for 2 h which finally produced ALP nanoparticles upon calcination at 900°C for 2 h in a Muffle furnace under air atmosphere. The furnace was allowed to cool by ambient cooling and fine ALP nanoparticles were obtained by grinding in a Mortar and Pestle.

Fabrication of SPEEK Composite Membrane

Pure SPEEK and composite membranes containing different types of fillers (viz. TPA, ALP, TPA and ALP in combination) were fabricated by solution casting of homogeneous solution on a Petri dish followed by slow evaporation of solvent to obtain dry composite film. Initially, homogeneous polymer solution was made by dissolving desired amount of SPEEK in DMAc solvent. The composite film containing 10 wt % TPA exhibited best proton conductivity. To investigate the effect of ALP on the functional properties of SPEEK/TPA membrane, SPEEK/TPA/ALP nanocomposite membranes consisting 3, 5, 10 wt % of ALP nanoparticles were fabricated in similar ways keeping TPA loading constant at optimum concentration (i.e., 10 wt %). The

Table I. Sample designation

Sample code	TPA (wt %)	ALP (wt %)
SPEEK	-	-
SPEEK/TPA5	5	-
SPEEK/TPA10	10	-
SPEEK/TPA25	25	-
SPEEK/TPA50	50	-
SPEEK/ALP3	-	3
SPEEK/ALP5	-	5
SPEEK/ALP10	-	10
SPEEK/TPA10/ALP3	10	3
SPEEK/TPA10/ALP5	10	5
SPEEK/TPA10/ALP10	10	10

detailed compositions of composite membranes are shown in Table I.

CHARACTERIZATION

X-ray diffraction (XRD) pattern of synthesized nanoparticles, PEEK and SPEEK were recorded in Rigaku Miniflex 600. The samples were scanned from 10 to 70° at the scan rate of 0.02° s^{-1} using Cu Kα radiation at ambient temperature.

Attenuated total reflectance (ATR)-Fourier Transform Infrared (FTIR) Spectroscopy analysis of PEEK and synthesized SPEEK was carried out in Tensor 27 FTIR instrument (Bruker, Germany). The samples were scanned from 600 to 4000 cm^{-1} to investigate the functional groups present in the polymer backbone.

The IEC of composite films was determined by titration using eq. (1). Prior to testing the membranes were dipped in NaCl solution for exchanging protons with Na^+. Finally, H^+ ions released in solution were back titrated with standard NaOH solution. The IEC is expressed in $meqvg^{-1}$.

$$\text{IEC} = (\text{Consumed NaOH in ml} \times \text{Molarity of NaOH})/W_{\text{dry}} \quad (1)$$

where, W_{dry} is the weight of membrane in dry condition.

The ionic conductivity of composites was evaluated by AC impedance analysis of hydrated film in the frequency range of 20 Hz to 2 MHz using Agilent E4980A Precision LCR meter at room temperature. Proton conductivity of the composites was calculated by using eq. (2).

$$\sigma = L/(R \times S) \quad (2)$$

Where, σ denotes the proton conductivity in $S\ cm^{-1}$, L represents the thickness in cm, R is the membrane resistance in ohm, and S represents the area of membrane in cm^2.

Thickness and area of the membranes for conductivity measurement were in the range of 0.052 ± 0.008 cm and 1.13 cm^2. Bulk resistance of each membrane was calculated from the high frequency zone of impedance curves by nonlinear curve fitting using equation of semicircle and used further to calculate the proton conductivity.

Water uptake of composite films was checked by taking the weight difference between completely dried and wet films. Completely dried membranes were first immersed in deionized water until constant weight was achieved. Water uptake was then calculated using eq. (3).

$$\text{Water uptake} = (W_{\text{wet}} - W_{\text{dry}}) \times 100/W_{\text{dry}} \quad (3)$$

where, W_{wet} and W_{dry} represent the wet and dry weight of films.

Thermal stability of the composite films and SPEEK were determined in Pyris Diamond TG/DTA instrument. The samples were heated from room temperature to 700°C under nitrogen atmosphere at a heating rate of 10°C min^{-1}. Thermal transition of the ALP nanoparticles was studied in a Perkin Elmer Pyris Diamond differential scanning calorimeter (DSC) by heating the nanoparticles from 50 to 200°C temperature at a rate of 10°C min^{-1} under nitrogen atmosphere.

Rate of desorption of water from composite films was determined by isothermally heating the samples at 60°C for 1 h in TGA instrument. The film samples were first immersed in deionized water until constant weight was attained. After quick removal of surface water, the films were placed in TG/DTA instrument for isothermal heating. The rate of dehydration of composite films was evaluated by plotting M_t/M_0 with respect to time (t). Where, M_t denotes the amount of water remains in film at any time t and M_0 represents the initial water content of the film. The slope of initial linear portion of M_t/M_0 versus t plot gives the rate of dehydration of membranes at said temperature.

Leaching of conductive filler (TPA) from the electrolyte membrane is one of the drawbacks of SPEEK/TPA based composites. The effect of ALP nanoparticles on the extent of leaching of conductive TPA was observed by UV–vis spectroscopy. The composite membranes were dipped in equal volume of water for 4 days to allow the fillers to leach out from the composite films and then extracted solutions were taken for further analysis in spectrometer.

Microstructure of the composites was examined in Scanning Electron Microscope (SEM), Quanta 200, Zeiss, Germany.

RESULTS AND DISCUSSION

X-ray Diffraction

Figure 1(a) indicates the XRD pattern of synthesized ALP nanoparticles. It shows most intense peak at 2θ value of 20.71° due to diffraction at (020) plane and other characteristic peaks at 2θ value of 21.67°, 23.26°, 27.38°, 29.87°, 35.73°, 38.80°, 42.09°, 42.93°, 53.72°, 55.84°, 57.11°, 59.97°, and 64.03° corresponds to diffraction at (211), (212), (301), (124), (107), (410), (041), (325), (2010), (435), (054), (0310), and (615) crystal planes, respectively. XRD pattern of the nanoparticles conforms well to the database (JCD file no. 1403729 (1992), 97, 163–168) and confirms the presence of crystalline ALP phase within the nanoparticles. Average crystallite size (D) of nanoparticles is evaluated considering the most intense peak by using Scherrer equation [Eq. (4)].

$$D = k\lambda/\beta\cos\theta \quad (4)$$

where, k represents Scherrer constant (generally taken as 0.9), λ indicates wavelength of X-ray radiation in nm, β is the full

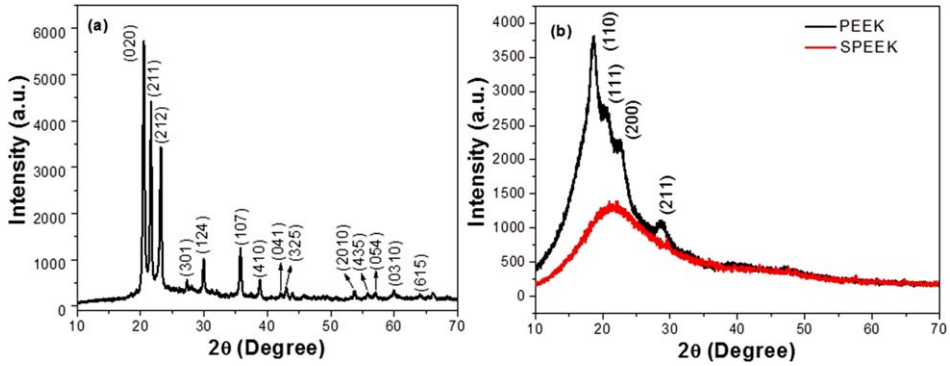

Figure 1. X-ray pattern of (a) ALP nanoparticles, (b) PEEK and SPEEK membranes. [Color figure can be viewed in the online issue, which is available at wileyonlinelibrary.com.]

angular line width in radians at half maximum intensity and θ represents diffraction angle in degree.

The average crystallite size of nanoparticles calculated by using the above equation appears to be ~62 nm, which matches well with the particle size obtained from the SEM image.

Figure 1(b) denotes the XRD pattern of PEEK and synthesized SPEEK. PEEK shows XRD peaks at 18.71°, 20.65°, 22.68°, and 28.69° due to its semi-crystalline nature. These peaks can be ascribed to the diffraction at (110), (111), (200), and (211) crystalline planes of PEEK, respectively. Introduction of $-SO_3H$ group reduces the crystallinity of PEEK due to restriction imparted by the functional groups in ordered packing of polymeric chains. Thus intensity of (110) peak is reduced in SPEEK accompanying with relative broadening. Other crystalline peaks are not observed in SPEEK due to disruption of crystalline structure.

ATR-FTIR Analysis

Figure 2 exhibits the ATR-FTIR spectra of PEEK and SPEEK. IR absorption bands at 1044 and 1267 cm^{-1} appear owing to incorporation of $-SO_3H$ groups in the main polymer backbone.[32] Appearance of new absorption peaks at 1044 and 1267 cm^{-1} can be ascribed to the asymmetric stretching vibration of O=S=O linkage in $-SO_3H$ group.[33] Absorption band at 1163 cm^{-1} can be attributed to the in plane bending vibration of C–H bond in $-CH_3$ group. IR bands at 1398 and 1495 cm^{-1} can be designated to the C–C stretching vibration, while IR peaks at 1587 and 1630 cm^{-1} appear due to C=C stretching vibration of aromatic ring. Strong peaks at 978 and 1773 cm^{-1} can be attributed to the C–H in plane bending of aromatic ring and C=O stretching vibration of ketone linkages.

Degree of Sulfonation

Figure 3 denotes the TGA thermogram of virgin SPEEK membrane. DS of SPEEK is determined from the weight loss in TGA thermogram corresponding to the desulfonation step using eq. (5)[34]

$$\mathrm{DS} = \text{Molecular weight of } M(\mathrm{PEEK}) / [(m/\Delta m) - 1] \times M(-SO_3H) \quad (5)$$

where M (PEEK) and M ($-SO_3H$) represent molecular mass of PEEK and $-SO_3H$ group. m is mass of SPEEK at the starting of desulfonation process and Δm is the weight sacrifice due to desulfonation. Experimentally determined value of DS comes out to be 76%

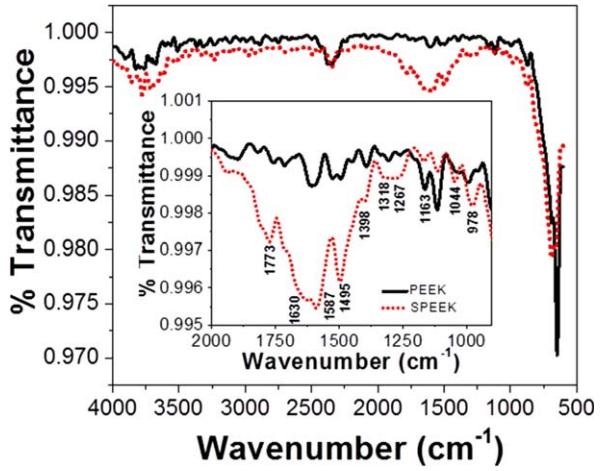

Figure 2. ATR-FTIR spectra of PEEK and SPEEK. [Color figure can be viewed in the online issue, which is available at wileyonlinelibrary.com.]

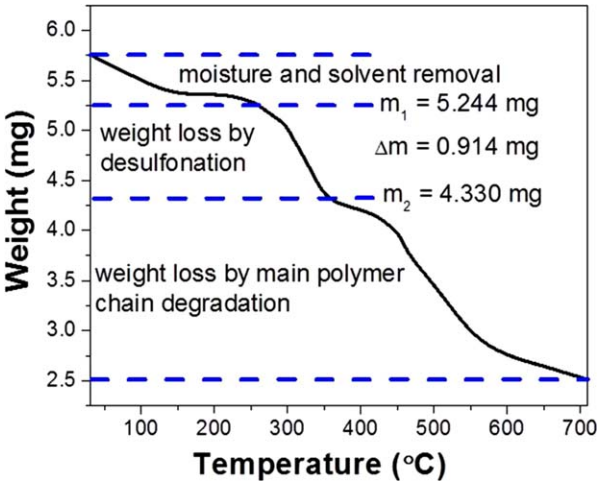

Figure 3. TGA thermogram of SPEEK. [Color figure can be viewed in the online issue, which is available at wileyonlinelibrary.com.]

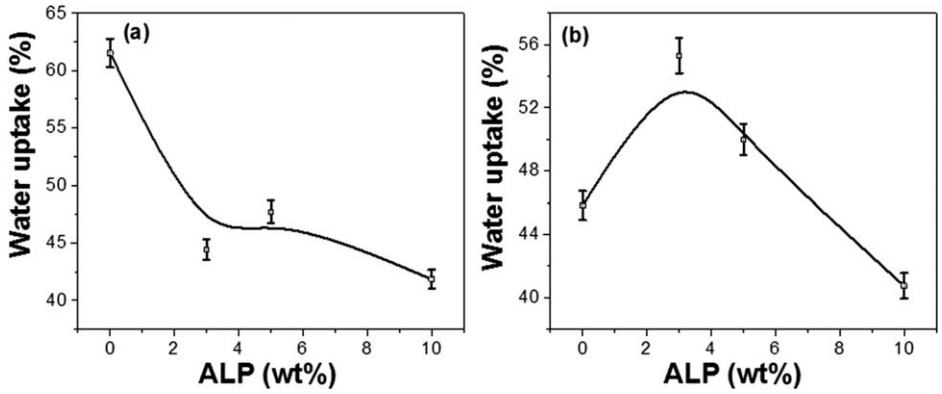

Figure 4. Water uptake capacity of (a) SPEEK/ALP and (b) SPEEK/TPA10/ALP composite films with respect to filler loading.

Water Uptake Capacity

Determination of water uptake of PEMs is an important parameter due to water dependent proton conductivity of composite membranes. Water uptake of SPEEK/TPA composite membranes is observed to be decreased with the rise in concentration of TPA. SPEEK absorbs water due to the presence of strong hydrophilic $–SO_3H$ groups. Therefore, the decrease in water uptake capacity of composite membranes can be attributed to the reduction in numbers of $–SO_3H$ groups with increasing TPA loading. Moreover, the ionic interaction between TPA and $–SO_3H$ groups of SPEEK also decreases the water uptake capacity of composite membranes as $–SO_3H$ groups are engaged by this specific interaction.[35–37] Figure 4(a) represents the water uptake of SPEEK/ALP composite membranes as a function of ALP loading. SPEEK/ALP membranes exhibit a decreasing trend in water uptake capacity with the increase in ALP loading. This might be because of reduction in number of $–SO_3H$ groups (i.e., SPEEK content) with increase in ALP loading. Figure 4(b) depicts the water uptake behavior of SPEEK/TPA/ALP composite membranes with respect to ALP loading at fixed concentration of TPA (10 wt %). It is observed that the water uptake capacity of SPEEK/TPA/ALP composite membranes increases rapidly up to 3 wt % ALP loading. This sudden rise in water uptake capacity may be attributed to the reduction of strong ionic interaction between $–SO_3H$ group of SPEEK and TPA in presence of ALP. With further increase in ALP loading, water uptake of SPEEK/TPA/ALP composite membranes shows a general decreasing trend due to increase in mass transfer resistance for water penetration. Composite films form dense microstructure at higher filler loading and thus offer grater resistance to water penetration. Hence at 10 wt % ALP loading water uptake becomes almost comparable as that of SPEEK/ALP10 composite.

Ion Exchange Capacity

The IEC is another important parameter to assess the performance of PEMs. Addition of HPA generally decreases the IEC of SPEEK/HPA composite membranes due to the strong ionic interaction between SPEEK and HPAs.[38] Figure 5(a) depicts the IEC of SPEEK/ALP composite membranes as a function of ALP content. It is observed that the composite membranes exhibit an initial fall in IEC up to 3 wt % ALP loading and then show a rise in IEC value with further increase in filler loading. At 10 wt % ALP loading IEC becomes almost equal to that of SPEEK. This may be attributed to the fact that addition of ceramic fillers (ALP) increases the density of membranes and thus the numbers of accessible acidic sites for mass transfer (i.e., proton exchange) process are reduced. Moreover, mobility of ions is restricted and exchange process becomes partially incomplete.[39] Therefore, an initial reduction in IEC of SPEEK/ALP composite membranes is observed when ALP nanoparticles loading is increased up to 3 wt %. At higher ALP loading, the interaction between SPEEK and ALP becomes unfavorable due to predominant intra-particle interaction.[40] Hence, phase separated morphology (one discontinuous SPEEK matrix and other cluster of filler particles) is developed in the composite membrane.

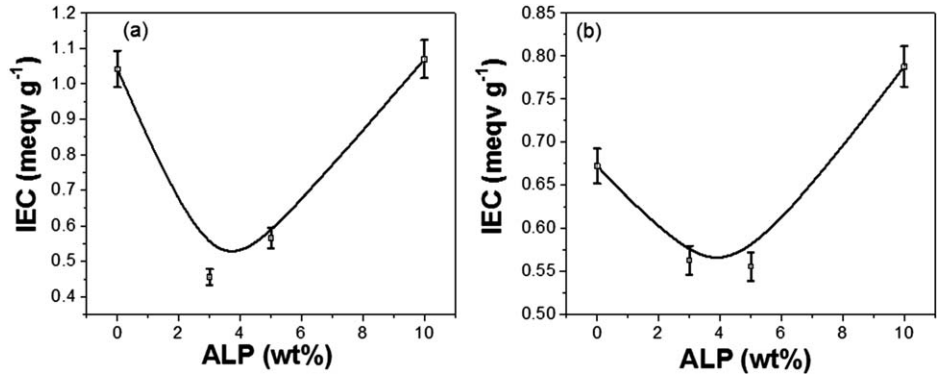

Figure 5. IEC of (a) SPEEK/ALP and (b) SPEEK/TPA10/ALP composite films as function of filler loading.

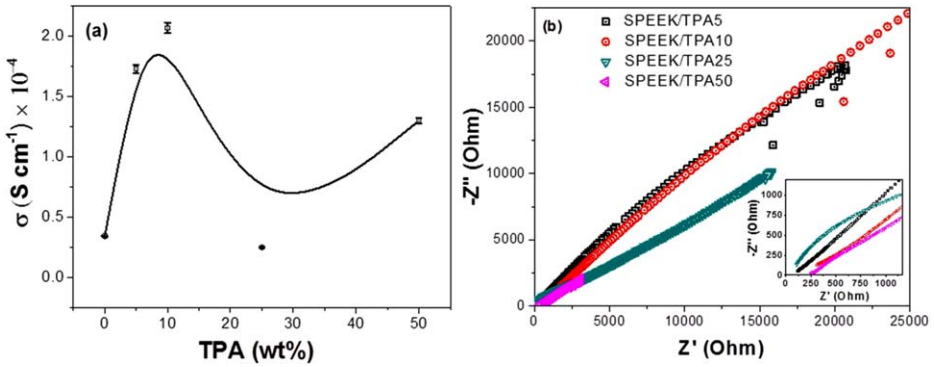

Figure 6. (a) Proton conductivity, (b) Nyquist plot of SPEEK/TPA composite membranes. [Color figure can be viewed in the online issue, which is available at wileyonlinelibrary.com.]

Therefore, SPEEK matrix becomes capable to participate more freely into the ion exchange process. Moreover, hydrophilic characteristic of ALP NPs also comes into effect at higher filler loading. Porous structure and hydrophilic nature of ALP favor retention of water within the composite membrane and ease ion exchange process by increasing the mobility of protons since water acts as a vehicle for proton transfer. Hence beyond 3 wt % ALP loading IEC of SPEEK/ALP membranes starts to rise again.

Figure 5(b) represents the IEC of SPEEK/TPA/ALP composite membranes with respect to ALP loading. It is observed that similar to SPEEK/ALP membranes SPEEK/TPA/ALP membranes also exhibit an initial fall in IEC up to 5 wt % ALP loading due restriction imparted by the ceramic filler in proton exchange process as described earlier. Further increase in ALP loading from 5 to 10 wt % increases the IEC of composite membranes. This can be attributed to the decrease in specific interaction between SPEEK and TPA in presence of high ALP content. Hence more protons of $–SO_3H$ groups can take part in ion exchange process due to ease in ionic mobility in presence of water (due to high water retention ability of hydrophilic ALP NPs). This phenomenon ultimately leads to increase in IEC of composite membranes.

Proton Conductivity

High proton conductivity is one of the prime requirements for PEMs to achieve an efficient fuel cell performance. HPAs are generally included as solid conducting filler with an aim to improve proton conductivity of polymer matrices. Addition of TPA within SPEEK is observed to improve the proton conductivity of composite membranes.[35–37] Figure 6(a) represents the conductivity plot and Figure 6(b) shows the corresponding Nyquist plot for SPEEK/TPA composite membranes. It is observed that proton conductivity increases up to 10 wt % TPA loading and then decreases beyond it. Therefore, 10 wt % TPA is found to be optimum filler loading and hence SPEEK/TPA10 composite membrane was taken as base material for preparation of SPEEK/TPA/ALP nanocomposite membranes.

Figure 7(a) and 7(b) represent proton conductivity plots, while Figure 7(c) and 7(d) exhibit corresponding Nyquist plots for SPEEK/ALP and SPEEK/TPA10/ALP composite membranes. SPEEK/ALP composite membranes exhibit an improvement in proton conductivity up to 3 wt % ALP loading due to the incorporation of hydrophilic filler within SPEEK matrix. ALP improves the water retention behavior of SPEEK and therefore composite membrane exhibits increased proton conductivity. At 5 and 10 wt % ALP loading the proton conductivity decreases compared to SPEEK/ALP3 membrane due to restriction imparted by ALP in proton mobility at high filler loading. In case of SPEEK/TPA/ALP composite membranes proton conductivity value reaches as high as 6.8×10^{-4} S cm^{-1} at 3 wt % ALP loading as shown in Figure 7 (b). The proton conductivity is even higher that of SPEEK/TPA10 and SPEEK/ALP3 composite membranes. Therefore use of TPA and ALP filler in combination synergized the proton conduction phenomena. Hence ~3.3 and ~1.7 times increment in proton conductivity is achieved in SPEEK/TPA10/ALP3 composite membrane compared to SPEEK/TPA10 and SPEEK/ALP3 composite membranes. Further increase in ALP loading decreases the proton conductivity of SPEEK/TPA/ALP composite membranes, which can be attributed to the restriction imparted by ceramic filler (ALP) in proton mobility at higher filler loading.

Thermal Analysis

Addition of TPA increases the thermal stability of composite films. This can be attributed to the ionic interaction of TPA molecules with $–SO_3H$ groups of SPEEK matrix. Higher the TPA content in composite membrane more is its thermal stability. This may be because of increased resistance to the heat transfer from superficial combustion zone to composite films with increasing filler loading. Moreover, it is worth mentioning that the SPEEK and composite membranes show three-step weight loss process. First weight loss takes place due to loss of absorbed moisture and solvent from the membrane. Second weight loss takes place at 260°C due to the removal of $–SO_3H$ groups of SPEEK matrix. Third major weight loss starts after 400°C and continued thereafter due to the main chain degradation of SPEEK. Table II summarizes the weight loss involved in different steps of the TGA thermogram of the membranes. Addition of TPA in SPEEK matrix increases the residue content at 700°C due to the incorporation of high molecular weight inorganic filler. Increase in TPA loading leads to progressively increased residue content in the composites. Figure 8(a)

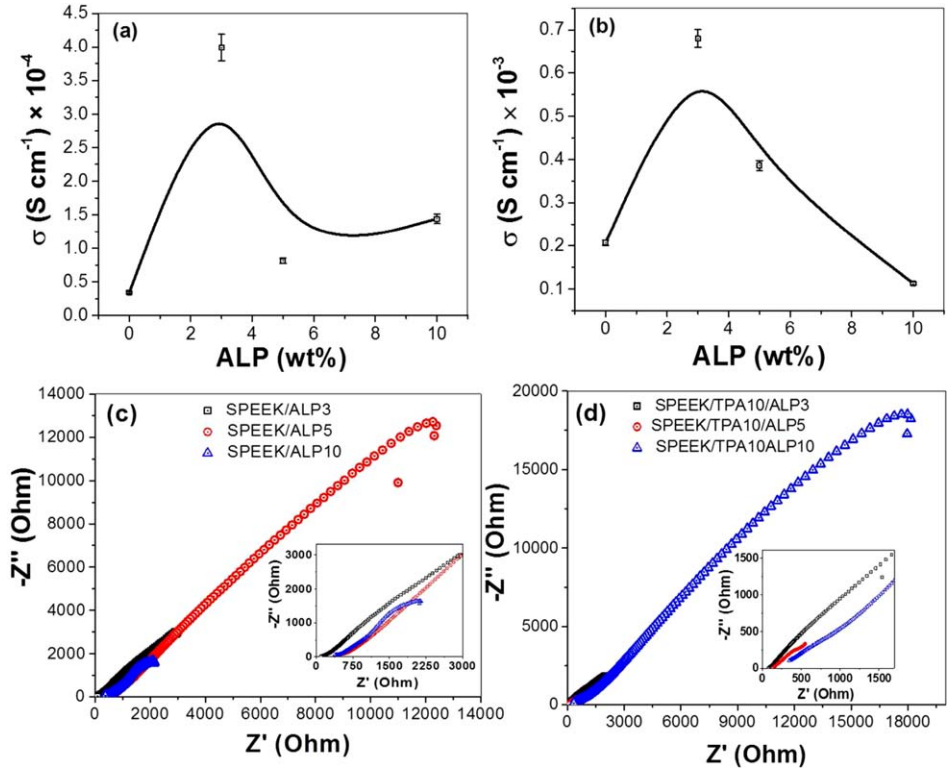

Figure 7. Proton conductivity of (a) SPEEK/ALP, (b) SPEEK/TPA10/ALP; Nyquist plots of (c) SPEEK/ALP, (d) SPEEK/TPA10/ALP composite membranes. [Color figure can be viewed in the online issue, which is available at wileyonlinelibrary.com.]

represents the effect of ALP on thermal stability of SPEEK and SPEEK/TPA10 composite membranes. Study reveals that the inclusion of ALP in SPEEK matrix decreases thermal stability of SPEEK membranes to some extent as evidenced by the decreased residue content in Table II. This can be attributed to the hydrophilic nature of ALP. Membranes show progressively increased weight loss up to 150°C due to loss of entrapped water molecules as shown in first step of TGA thermogram (See Table II). Figure 8(b) and inset of Figure 8(b) show TGA and differential scanning calorimetry (DSC) thermogram of ALP nanoparticles. TGA curve of ALP reveals that the calcined nanoparticles undergo about 20 % weight loss in the temperature range of 100–150°C due to presence of water molecules. DSC thermogram of ALP nanoparticles also exhibits thermal transition at around 90°C supporting the presence of sorbed water molecules within the nanoparticles.[41] Thermal stability of SPEEK/TPA10/ALP10 membrane is found to be intermediate between SPEEK/ALP10 and SPEEK/TPA10. This increased thermal stability of SPEEK/TPA10/ALP10 composite membrane compared to SPEEK/ALP10 membrane can be attributed to the presence of TPA within it. All the composite membranes are thermally stable up to 200°C, which is sufficient enough for the intended fuel cell membrane application.

Water Desorption Properties of Composite Membranes

For effective prolonged operation of fuel cell devices retention of water within the PEM is crucial. Addition of TPA increases the rate of desorption of water from composite films compared to pure SPEEK matrix. At 10 wt % TPA loading rate of water desorption is observed to attain its maximum value. This can be attributed to the fact that, 10 wt % being the optimum concentration of TPA large amount of water is available in the membrane due to hygroscopic nature of TPA. Hence, composite films absorb more moisture due to presence of TPA within it.

Table II. Weight loss in different steps of TGA thermogram

Sample code	Weight loss in Step 1 (%)	Weight loss in Step 2 (%)	Weight loss in Step 3 (%)	Residue (%)
SPEEK	8.72	16.74	30.62	43.92
SPEEK/TPA10	5.61	16.12	24.55	53.72
SPEEK/ALP 10	12.92	16.35	27.98	42.75
SPEEK/TPA 10/ALP3	10.69	15.12	20.32	53.87
SPEEK/TPA 10/ALP5	11.00	15.57	20.31	53.12
SPEEK/TPA 10/ALP10	11.15	16.69	22.5	49.66

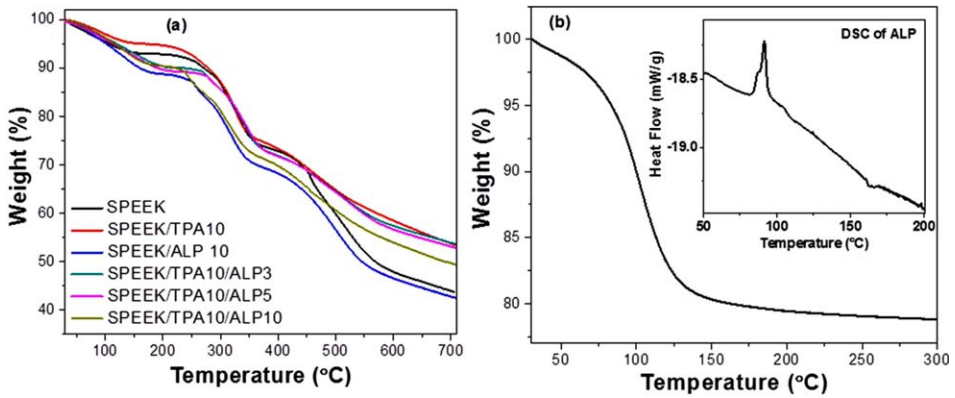

Figure 8. TGA thermogram of (a) SPEEK/ALP and SPEEK/TPA10/ALP composite films; (b) TGA and DSC thermogram of ALP nanoparticles. [Color figure can be viewed in the online issue, which is available at wileyonlinelibrary.com.]

Moreover, TPA contains 25 H_2O molecules within its crystal structure which are also responsible for higher water desorption rate of the composite films since rate of desorption depends on the water content of membrane.[42,43]

Figure 9(a) depicts the M_t/M_0 versus time plot and Figure 9(b) represents corresponding water desorption rate as a function of ALP loading for SPEEK/ALP composite films. Figure 9(b) indicates that ALP alone shows slight increase in the rate of desorption of SPEEK membranes. Hydrophilic nature of ALP helps composite membrane to absorb water molecules within it and hence higher desorption rate is observed with increasing ALP loading. Moreover, hydrophilic nature of ALP is further supported by high initial weight loss of ALP in TGA thermogram [See Figure 8(b)]. Use of ALP in combination with TPA is found to exhibit remarkable reduction in the rate of dehydration of SPEEK/TPA/ALP composite membranes as shown in Figure 9(c) and (d). Incorporation of ALP effectively reduces the rate of desorption of SPEEK/TPA10 composite membranes and hence SPEEK/TPA10/ALP composite membranes show gradually decreased water desorption rate with increasing ALP loading. This may be because of synergistic effect of TPA and ALP on the water retention ability of composite films. ALP retains water within its porous structure and therefore water

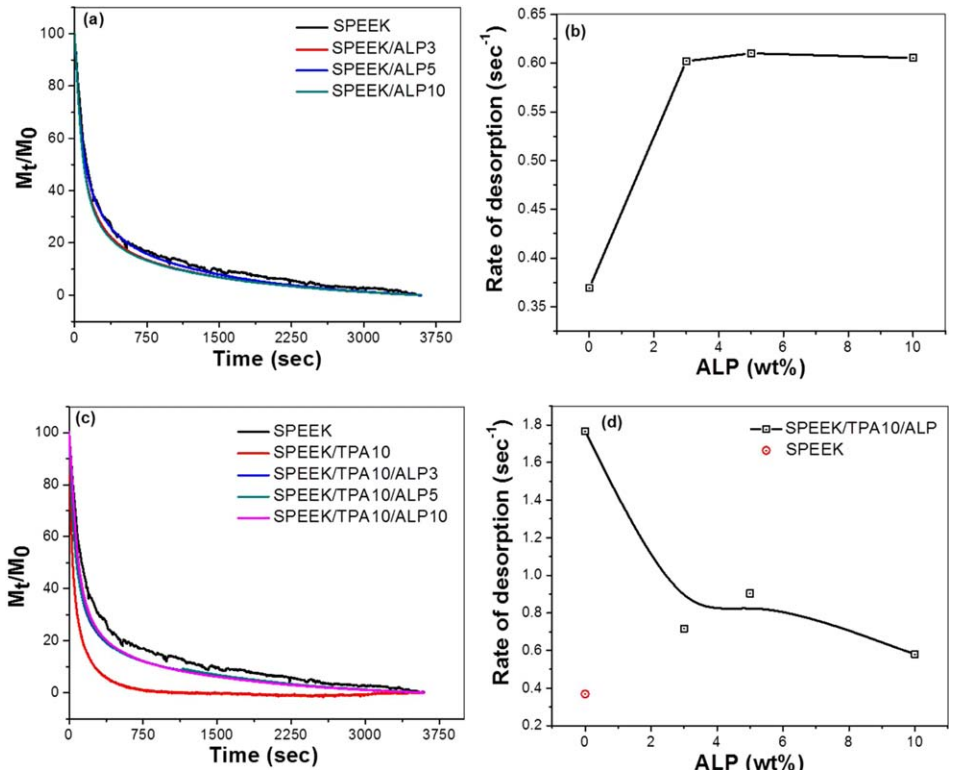

Figure 9. (a) M_t/M_0 versus t plot and (b) Rate of desorption *vs.* ALP loading plot of SPEEK and SPEEK/ALP composite, (c) M_t/M_0 versus t plot and (d) Rate of desorption *vs.* ALP loading plot of SPEEK and SPEEK/TPA10/ALP composite films. [Color figure can be viewed in the online issue, which is available at wileyonlinelibrary.com.]

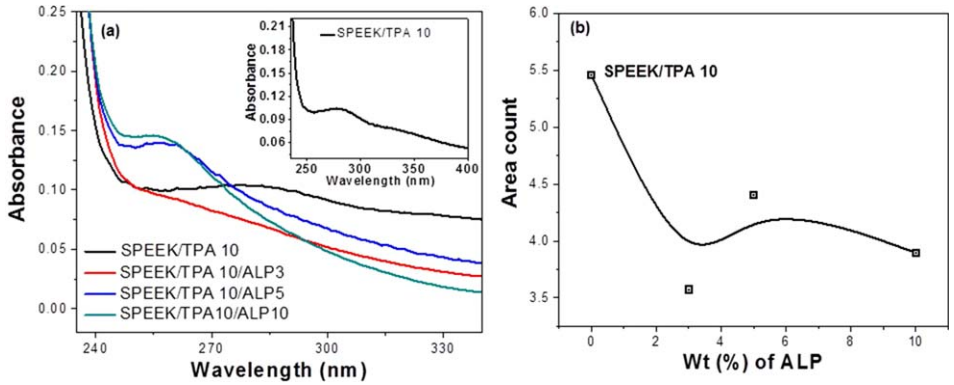

Figure 10. (a) UV-vis spectrogram of SPEEK/TPA10 and SPEEK/TPA10/ALP membranes, (b) Integrated area counts *vs.* wt % of ALP. [Color figure can be viewed in the online issue, which is available at wileyonlinelibrary.com.]

molecule has to travel more tortures path before escaping from the composite membrane and hence significant reduction in water desorption rate is observed. Retention of water within polymeric membrane by the inorganic phosphates was also reported in earlier work.[44] However, the effect of phosphates on the physicochemical properties of electrolyte membranes was not studied yet. Hence this study reports the effect of ALP on the retention behavior of SPEEK membrane in detail.

Quantitative Estimation of Leaching of TPA by UV–Vis Spectroscopy

Figure 10(a) represents the UV–vis spectra of SPEEK/TPA10 and SPEEK/TPA10/ALP composite membranes. The amount of filler leached from PEM in a fixed volume of water is measured in spectrophotometer. The characteristic UV–vis peak for pure TPA appears at 280 nm which somehow shifted to around 258 nm in case of leached aqueous solution as evidenced in Figure 10(a). Inset of Figure 10(a) shows UV-*vis* spectra of TPA leached out from SPEEK/TPA10 composite membrane. The absorption peaks are observed at around 280 and 340 nm due to the presence of W=O and W–O–W covalent bonds in Keggin's structure of TPA. The conductive filler leached out from SPEEK/TPA/ALP composite films exhibits absorption peaks at somehow lower value due to blue shift in the wavelength. The blue shift may be attributed to the strong interaction between TPA and ALP nanoparticles arising from the uniform dispersion of ALP nanoparticles and TPA within the polymer matrix. Since absorption energy of quantum dots varies inversely with radius hence, lower is the diameter of nanoparticles, absorption peak shifts more towards the lower wavelength region. Therefore, it is evidenced from the absorption peak positions (for leached solution of SPEEK/TPA/ALP composite films) that particle size of

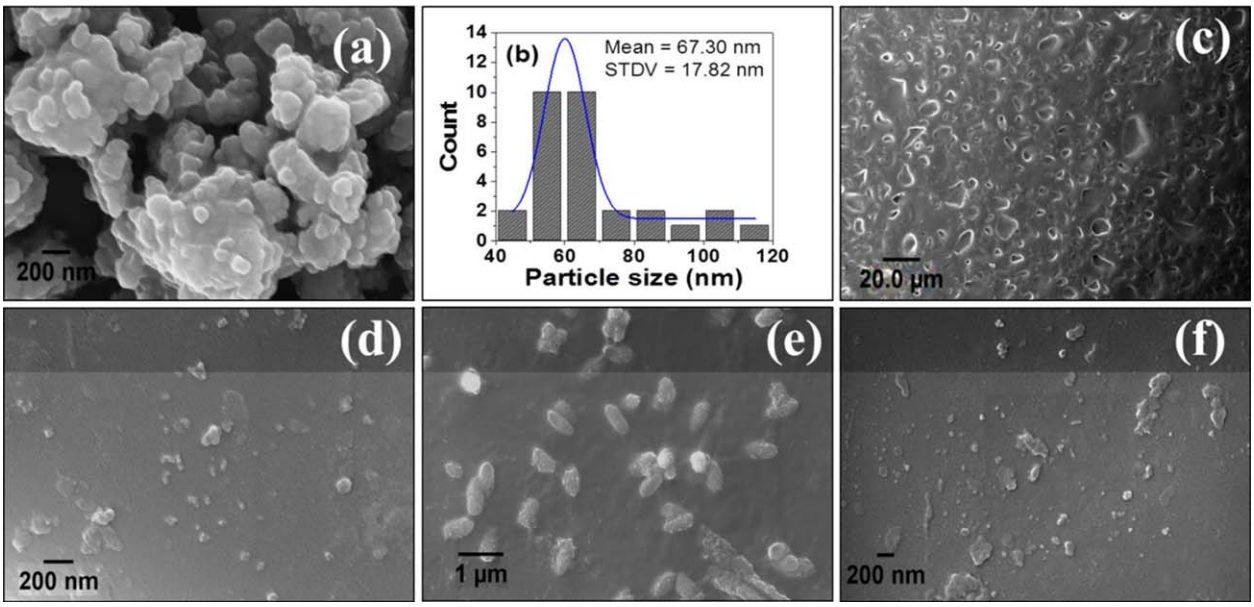

Figure 11. SEM images of (a) ALP nanoparticles, (b) particle size histogram of ALP nanoparticles, (c) SPEEK/ALP10 (at low magnification), (d) SPEEK/ALP10 (at high magnification), (e) SPEEK/TPA10, (f) SPEEK/TPA10/ALP10 composite films. [Color figure can be viewed in the online issue, which is available at wileyonlinelibrary.com.]

filler in SPEEK/TPA/ALP matrix remains much smaller and well distributed compared to SPEEK/TPA composite membranes.[45]

The amount of TPA leached in water was calculated by integrating area under the absorption peak. Effect of ALP on leaching of TPA is plotted in Figure 10(b). The leaching of TPA is observed to be lower for SPEEK/TPA/ALP membranes compared to SPEEK/TPA membranes. The lowest area count is obtained in case of SPEEK/TPA10/ALP3 indicating maximum stability of TPA against water leaching among all SPEEK/TPA10/ALP nanocomposites. This may be attributed to the strong chemical linkage between TPA and ALP nanoparticles.[43] The leaching of TPA from SPEEK/TPA10/ALP3 nanocomposite membrane is reduced by 34.5% as compared to SPEEK/TPA10 membrane.

Morphology

Figure 11(a) shows the SEM image and Figure 11(b) represents the corresponding particle size histogram of ALP nanoparticles used for preparation of composite membranes. It is observed that ALP nanoparticles in bulk exist as agglomerated clusters due to the strong van der Waals forces of attraction existing among the nanoparticles. The average particle size of the ALP nanoparticles is 67.30 nm with standard deviation of 17.82 nm. The particle size matches well with the crystallite size determined by Sherrer equation (~62 nm). Figure 11(c) and 11(d) represent the morphology of SPEEK/ALP10 films at two different magnifications (viz. 20 μm and 200 nm). Figure 11(c) depicts that SPEEK/ALP10 shows porous microstructure throughout its film surface. Hence, higher water desorption rate may be because of the presence of large amount of entrapped water within these pores. Figure 11(d) shows that ALP nanoparticles form small clusters and homogeneously distributed within the SPEEK matrix at 10 wt % filler loading. Figure 11(e) demonstrates the morphology of SPEEK/TPA composite membrane at 10 wt % TPA content. It is observed that SPEEK/TPA10 exhibits uniform distribution of filler within the SPEEK matrix. Figure 11(f) shows the SEM image of SPEEK/TPA10/ALP10 composite films. It shows that TPA and ALP nanoparticles form small agglomerates within the SPEEK matrix.

CONCLUSIONS

Present research work explores the synergistic effect of TPA and ALP on the fuel cell properties of SPEEK membrane. Use of TPA and ALP together in SPEEK matrix leads to improved membrane properties compared to individual TPA or ALP filled SPEEK. SPEEK/TPA10 membrane shows the best performance among composite membranes filled with different percentage of TPA. However, synergistic effect in proton conductivity, water uptake and water desorption rate is observed in SPEEK/TPA10/ALP3 composite membrane. Addition of ALP in SPEEK/TPA membrane remarkably increases retention of water within the composite membrane. The composite membranes possess thermal stability up to 200°C which is sufficient enough for the intended fuel cell application. ALP nanoparticles also effectively reduce leaching of TPA from the composite membrane. Hence membrane can be used for longer time without much reduction in proton conductivity. Therefore SPEEK/TPA/ALP nanocomposite could be the promising PEM materials for future fuel cell application.

ACKNOWLEDGMENTS

Authors acknowledge Department of Science & Technology, Government of India for providing the fellowship for this work.

REFERENCES

1. Tripathi, B. P.; Shahi, V. K. *Prog. Polym. Sci.* **2011**, *36*, 945.
2. Hongwei, Z.; Fei, Y.; Danying, Z. *J. Appl. Polym. Sci.* **2013**, *130*, 4581.
3. Lufrano, F.; Squadrito, G.; Patti, A.; Passalacqua, E. *J. Appl. Polym. Sci.* **2000**, *77*, 1250.
4. Banerjee, S.; Kar, K. K.; Ghorai, M. K.; Das, S. *High Perform. Polym.* **2014**, *27*, 402.
5. Pramanik, S.; Kar, K. K. *J. Appl. Polym. Sci.* **2012**, *123*, 1100.
6. Liu, S.; Liu, Y.; Sang, S.; Zhong, W.; Wu, Q. *J. Appl. Polym. Sci.* **2015**, *132*, 41946.
7. Sinirlioglu, D.; Celik, S. U.; Muftuoglu, A. E.; Bozkurt, A. *J. Appl. Polym. Sci.* **2014**, *131*, 40107.
8. Hu, Z.; He, G.; Gu, S.; Liu, Y.; Wu, X. *J. Appl. Polym. Sci.* **2014**, *131*, 39852.
9. Mohtar, S. S.; Ismail, A. F.; Matsuura, T. *J. Membr. Sci.* **2011**, *371*, 10.
10. Carbone, A.; Pedicini, R.; Sacca, A.; Gato, A.; Passalacqua, I. *E. J. Power Sources* **2008**, *178*, 661.
11. Colicchio, I.; Wen, F.; Keul, H.; Simon, U.; Moeller, M. *J. Membr. Sci.* **2009**, *326*, 45.
12. Gomes, A. S.; Filho, J. C. D. *Int. J. Hydrogen Energy* **2012**, *37*, 6246.
13. Lu, J. L.; Fang, Q. H.; Li, S. L.; Jiang, S. P. *J. Membr. Sci.* **2013**, *427*, 101.
14. Li, L.; Xu, L.; Wang, Y. *Mater. Lett.* **2003**, *57*, 1406.
15. Celso, F.; Mikhailenko, S. D.; Kaliaguine, S.; Duarte, U. L.; Mauler, R. S.; Gomes, A. S. *J. Membr. Sci.* **2009**, *336*, 118.
16. Kim, J-H.; Kim, S-K.; Nam, K.; Kim, D-W. *J. Membr. Sci.* **2012**, *415–416*, 696.
17. Nicotera, I.; Enotiadis, A.; Angjeli, K.; Coppola, L.; Gournis, D. *Int. J. Hydrogen Energy* **2012**, *37*, 6236.
18. Rangasamy, V. S.; Thayumanasundaram, S.; Greef, N. D.; Seo, J. W.; Locquet, J. -P. *Solid State Ionics* **2012**, *216*, 83.
19. Tripathi, B. P.; Kumar, M.; Shahi, V. K. *J. Membr. Sci.* **2009**, *327*, 145.
20. Banerjee, S.; Kar, K. K. *Recent Pat. Mater. Sci.* **2014**, *7*, 131.
21. Banerjee, S.; Kar, K. K.; Das, M. K. *Recent Pat. Mater. Sci.* **2014**, *7*, 1.
22. St-Arnaud, M.; Bebin, P. W. O. Patent, 2003083985, December 16, **2004**.
23. Vona, M. L.; Di, Sgreccia, E.; Donnadio, A.; Casciola, M.; Chailan, J. F.; Auer, G.; Kanuth, P. *J. Membr. Sci.* **2011**, *369*, 536.

24. Tominaga, Y.; Hong, I. C.; Asai, S.; Sumita, M. *J. Power Sources* **2007**, *171*, 530.
25. Ye, Y. S.; Liang, G. W.; Chen, B. H.; Shen, W. C.; Tseng, C. Y.; Cheng, M. Y.; Rick, J.; Huang, Y. J.; Chang, F. C.; Hwang, B. J. *J. Power Sources* **2011**, *196*, 5408.
26. Devrim, Y.; Erkan, S.; Bac, N.; Eroglu, I. *Int. J. Hydrogen Energy* **2012**, *37*, 16748.
27. Shao, Z. -G.; Joghee, P.; Hsing, I. -M. *J. Membr. Sci.* **2004**, *229*, 43.
28. Staiti, P.; Arico, A. S.; Baglio, V.; Lufrano, F.; Passalacqua, E.; Antonucci, V. *Solid State Ionics* **2001**, *145*, 101.
29. Carbone, A.; Casciola, M.; Cavalaglio, S.; Costantino, U.; Ornelas, R.; Fodale, I.; Saccà, A.; Passalacqua, E. *J. New Mater. Electrochem. Syst.* **2004**, *7*, 1.
30. Liu, G.; Jia, M.; Zhou, Z.; Wang, L.; Zhang, W.; Jiang, D. *J. Colloid Interface Sci.* **2006**, *302*, 278.
31. Zaidi, S. M. J.; Mikhailenko, S. D.; Robertson, G. P.; Guiver, M. D.; Kaliaguine, S. *J. Membr. Sci.* **2000**, *173*, 17.
32. Muthu Lakshmi, R. T. S.; Choudhary, V.; Varma, I. K. *J. Mater. Sci.* **2005**, *40*, 629.
33. El-Araby, R.; Attia, N. K.; Eldiwani, G.; Khafagi, M. G.; Sobhi, S.; Mostafa, T. *World Appl. Sci. J.* **2014**, *32*, 2239.
34. Knauth, P.; Hou, H.; Bloch, E.; Sgreccia, E.; Di Vona, M. L. *J. Anal. Appl. Pyrolysis* **2011**, *92*, 361.
35. Jang, I.-Y.; Kweon, O.-H.; Kim, K.-E.; Hwang, G.-J.; Moon, S.-B.; Kang, A.-S. *J. Membr. Sci.* **2008**, *322*, 154.
36. Baradie, B.; Poinsignon, C.; Sanchez, J. Y.; Piffard, Y.; Vitter, G.; Bestaoui, N.; Foscallo, D.; Denoyelle, A.; Delabouglise, D.; Vaujany, M. *J. Power Sources* **1998**, *74*, 8.
37. Kim, Y. S.; Wang, F.; Hickner, M.; Zawodzinski, T. A.; McGrath, J. E. *J. Membr. Sci.* **2003**, *212*, 263.
38. Dogan, H.; Inan, T. Y.; Unveren, E.; Kaya, M. *Int. J. Hydrogen Energy* **2010**, *35*, 7784.
39. Scipioni, R.; Gazzoli, D.; Teocoli, F.; Palumbo, O.; Paolone, A.; Ibris, N.; Brutti, S.; Navarra, M. A. *Membranes* **2014**, *4*, 123.
40. Ash, B. J.; Siegel, R. W.; Schadler, L. S. *J. Polym. Sci: Part B: Polym. Phys.* **2004**, *42*, 4371.
41. Yang, H.; Walton, R. I.; Biedasek, S.; Antonijevic, S.; Wimperis, S.; Ramirez-Cuesta, A. J.; Li, J.; Kolesnikov, A. I. *J. Phys. Chem. B* **2005**, *109*, 4464.
42. Fournier, M.; Feumi-Jantou, C.; Rabia, C.; Herve, G.; Launay, S. *J. Mater. Chem.* **1992**, *2*, 971.
43. Armatas, G. S.; Katsoulidis, A. P.; Petrakis, D. E.; Pomonis, P. J. *J. Mater. Chem.* **2010**, *20*, 8631.
44. Zaidi, S. M. *J. Electrochim. Acta* **2005**, *50*, 4771.
45. Yang, X. K.; Chen, L. F.; Wang, J. A.; Noreña, L. E.; Novaro, O. *Catalysis Today* **2009**, *148*, 160.